J. Fluid Mech. (2000), *vol.* 407, *pp.* 145–166. Printed in the United Kingdom

Turbulent diffusion near a free surface

By LIAN SHEN[1], GEORGE S. TRIANTAFYLLOU[2] AND DICK K. P. YUE[1]†

[1] Department of Ocean Engineering, Massachusetts Institute of Technology, Cambridge, MA 02139, USA

[2] Department of Naval Architecture and Marine Engineering, National Technical University of Athens, Zografou 15773, Athens, Greece

(Received 5 April 1999 and in revised form 22 October 1999)

We study numerically and analytically the turbulent diffusion characteristics in a low-Froude-number turbulent shear flow beneath a free surface. In the numerical study, the Navier–Stokes equations are solved directly subject to viscous boundary conditions at the free surface. From an ensemble of such simulations, we find that a boundary layer develops at the free surface characterized by a fast reduction in the value of the eddy viscosity. As the free surface is approached, the magnitude of the mean shear initially increases over the boundary (outer) layer, reaches a maximum and then drops to zero inside a much thinner inner layer. To understand and model this behaviour, we derive an analytical similarity solution for the mean flow. This solution predicts well the shape and the time-scaling behaviour of the mean flow obtained in the direct simulations. The theoretical solution is then used to derive scaling relations for the thickness of the inner and outer layers. Based on this similarity solution, we propose a free-surface function model for large-eddy simulations of free-surface turbulence. This new model correctly accounts for the variations of the Smagorinsky coefficient over the free-surface boundary layer and is validated in both *a priori* and *a posteriori* tests.

1. Introduction

The interaction of turbulence with a free surface is a problem essential to many applications, from air–sea interactions and transports to sensing of ship wakes. While a direct approach to these problems is still a formidable task, understanding the fundamental mechanism of turbulent diffusion near a free surface can facilitate considerably theoretical modelling and numerical simulations of the actual problems.

The turbulent diffusion near a free surface has been studied in the past by Hunt (1954), Ellison (1960), Levich (1962), Jobson & Sayre (1970), Davis (1972), Lee & Gill (1977), and Ueda *et al.* (1977). More recently there has been renewed interest in the problem of free-surface turbulence spurred by the availability of high-resolution numerical simulations and state-of-the-art experimental techniques. Numerical simulations of free-surface turbulence have been performed, for example, by Lam & Banerjee (1988), Handler *et al.* (1991, 1993), Leighton *et al.* (1991), Swean *et al.* (1991), Borue, Orszag & Staroselsky (1995), Dimas & Triantafyllou (1995), Pan & Banerjee (1995), Perot & Moin (1995), and Walker, Leighton & Garza-Rios (1996); while experimental measurements were obtained by Komori *et al.* (1982), Komori,

† Author to whom correspondence should be addressed.

Murakami & Ueda (1989), Nakagawa & Nezu (1981), Rashidi & Banerjee (1988, 1990), Gharib, Dabiri & Zhang (1994), Rashidi (1997), among many others.

In general, the free surface influences the evolution of turbulence in the flow through two effects: (*a*) the kinematic restriction of not allowing complete freedom for motions along the vertical direction; and (*b*) the vanishing of stresses at the free surface. It is now understood that, near the free surface, turbulence intensity in the horizontal plane is increased at the expense of that in the vertical direction. Furthermore, very near the free surface, vortex filaments attach to the free surface almost perpendicularly, with considerable dissipation of enstrophy. The first effect is attributed primarily to the kinematic boundary condition at the free surface which reduces the vertical velocity fluctuations. The second effect is attributed to the dynamic zero-stress condition. Both properties can be characterized as 'generic' of free-surface turbulence in the sense that they have been observed in all different types of free-surface turbulence flows. One can therefore loosely talk of a 'free-surface boundary layer' as a region of the flow with properties dominated by the effect of the free surface.

In a recent work (Shen *et al.* 1999), the features of a free-surface turbulent shear flow in the near-surface region are examined in detail including the distinction and elucidation of an outer 'blockage' layer and an inner 'surface layer' at the free surface. Shen *et al.* (1999), however, did not provide quantitative definitions of these free-surface layers, which are important to the modelling of the free-surface turbulence.

The main goal of the present paper is to *quantitatively* study the free-surface boundary layer in order to obtain insights necessary for turbulent modelling of free-surface flows. We use a combination of numerical simulation and theoretical analysis. Direct numerical simulation (DNS) is used to expound and quantify the free-surface turbulence boundary layer and also to confirm and calibrate the analytical solution. We adopt an eddy viscosity model and obtain an analytical similarity solution of the horizontally-averaged equation. The theoretical solution predicts well the surface layer behaviour obtained from DNS and is then used to predict the scaling properties of the boundary layer. The similarity solution also provides the basis for a new *free-surface function model* (FFM) for large-eddy simulation (LES) of free-surface turbulence.

The paper is organized as follows: in § 2 we provide the mathematical formulation for turbulent shear flow in the presence of a free surface. We outline the DNS implementation in § 3. The main DNS results are presented in § 4, which include the effects of the free surface on the mean shear and the eddy viscosity and the quantification of the free-surface layers. In § 5, we derive a similarity solution of the horizontally-averaged equation, confirm it against the DNS results, and use it to obtain scaling properties of the free-surface layers. As an application, we propose in § 6 a free-surface function model based on the similarity solution. The efficacy of this FFM for large-eddy simulation of free-surface turbulence is then demonstrated using both *a priori* and *a posteriori* tests. Finally in § 7, we present the conclusions.

2. Mathematical formulation

We consider a turbulent shear flow with a free surface at low Froude numbers. Referring to figure 1, the frame of reference has axes x, y, and z, where x and y are horizontal, z is vertical, positive upward, with the $z = 0$ plane coinciding with the undisturbed free surface. The mean shear is two-dimensional and is in the (x, z)-plane.

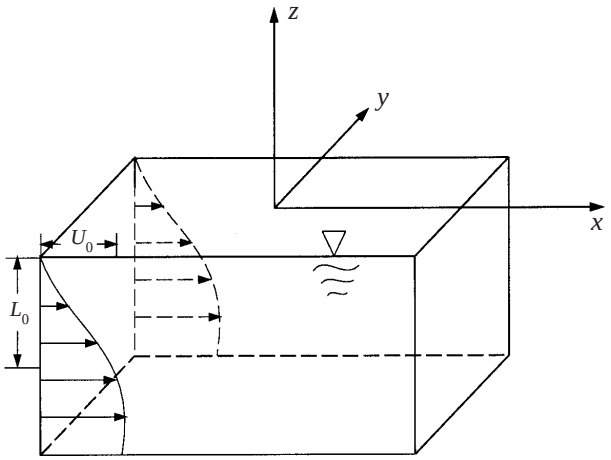

FIGURE 1. Schematic of a turbulent shear flow under a free surface.

The governing equations are the Navier–Stokes and continuity equations:

$$\frac{\partial u}{\partial t}+\frac{\partial uu}{\partial x}+\frac{\partial vu}{\partial y}+\frac{\partial wu}{\partial z}=-\frac{1}{\rho}\frac{\partial p}{\partial x}+\nu\left(\frac{\partial^2 u}{\partial x^2}+\frac{\partial^2 u}{\partial y^2}+\frac{\partial^2 u}{\partial z^2}\right), \tag{2.1}$$

$$\frac{\partial v}{\partial t}+\frac{\partial uv}{\partial x}+\frac{\partial vv}{\partial y}+\frac{\partial wv}{\partial z}=-\frac{1}{\rho}\frac{\partial p}{\partial y}+\nu\left(\frac{\partial^2 v}{\partial x^2}+\frac{\partial^2 v}{\partial y^2}+\frac{\partial^2 v}{\partial z^2}\right), \tag{2.2}$$

$$\frac{\partial w}{\partial t}+\frac{\partial uw}{\partial x}+\frac{\partial vw}{\partial y}+\frac{\partial ww}{\partial z}=-\frac{1}{\rho}\frac{\partial p}{\partial z}+\nu\left(\frac{\partial^2 w}{\partial x^2}+\frac{\partial^2 w}{\partial y^2}+\frac{\partial^2 w}{\partial z^2}\right), \tag{2.3}$$

$$\frac{\partial u}{\partial x}+\frac{\partial v}{\partial y}+\frac{\partial w}{\partial z}=0. \tag{2.4}$$

Here u, v, and w are the velocity components in x-, y-, and z- directions, respectively; p is the dynamic pressure, ρ the density, and ν the kinematic viscosity.

Consistent with the small Froude number flows, the free-surface elevation $h(x, y, t)$ is small and we linearize the free-surface boundary conditions as follows:

(i) Neglecting surface tension and modelling the air as a constant-pressure fluid layer, the balance of two tangential and one normal stress components at the free surface gives the dynamic boundary conditions:

$$\nu\left(\frac{\partial u}{\partial z}+\frac{\partial w}{\partial x}\right)=0 \quad \text{on } z=0, \tag{2.5}$$

$$\nu\left(\frac{\partial v}{\partial z}+\frac{\partial w}{\partial y}\right)=0 \quad \text{on } z=0, \tag{2.6}$$

$$p=2\rho\nu\frac{\partial w}{\partial z}+\rho g h \quad \text{on } z=0, \tag{2.7}$$

where g is gravitational acceleration.

(ii) The kinematic boundary condition is, upon Taylor expanding about $z=0$ and using (2.4),

$$w=\frac{\partial h}{\partial t}+\frac{\partial (uh)}{\partial x}+\frac{\partial (vh)}{\partial y} \quad \text{on } z=0. \tag{2.8}$$

3. Direct numerical simulations (DNS)

We start with an initial shear flow profile given by

$$\frac{U(z)}{U_0} = 1 - 0.9988\,\mathrm{sech}^2\left(0.88137\frac{z}{L_0}\right), \tag{3.1}$$

which is half of the mean velocity profile measured in the wake of a NACA 0003 hydrofoil in unbounded fluid (Mattingly & Criminale 1972). The Orr–Sommerfeld stability analysis of this velocity profile has been performed by Triantafyllou & Dimas (1989) and a detailed study on the nonlinear evolution of the instability is reported by Dimas & Triantafyllou (1994). Hereafter, all variables are normalized by the initial mean shear extent L_0 and the initial velocity deficit U_0.

In this study, the Froude number $Fr_0 \equiv U_0/\sqrt{gL_0}$ is 0.7, and we study three different initial Reynolds numbers $Re_0 \equiv U_0 L_0/\nu = 700$, 1000, 1400. For this small value of Fr_0, the effect of Froude number on the free-surface turbulence is proportionately small with the exception of pressure–strain effects (Shen *et al.* 1999). The effect of non-zero Froude number on free-surface turbulence statistics is examined in some detail in Shen *et al.* (1999) and will not be taken up here.

To simulate turbulence, we add a small divergence-free random velocity noise to the initial flow (3.1) and the simulation is carried out until a statistical steady-state condition is reached in the free-surface region.

Equations (2.1)–(2.4) subject to the free-surface boundary conditions (2.5)–(2.8) are solved numerically as an initial-boundary-value problem. The computational domain is closed by imposing periodic conditions on the four vertical boundaries far away, a free-surface boundary on the top, and a free-slip boundary on the (deep) bottom. The numerical method we use is based on a marker and cell method (Harlow & Welch 1965). We use a projection method which couples the Navier–Stokes equations and continuity equation to obtain a Poisson equation for the pressure with a divergence correction. The Poisson equation for pressure is solved at each sub-timestep. The simulation is advanced in time using an explicit second-order Runge–Kutta time integrator. A second-order finite-difference scheme at a staggered grid is used in the vertical direction wherein u, v, p are assigned at regular grids and w is assigned at staggered grids. In the horizontal directions, sixth-order finite-difference schemes are employed. Details of the numerical implementation can be found in Shen *et al.* (1999).

For later reference, in view of the statistical homogeneity in the horizontal directions, we use spatial averaging over the (x, y)-plane to define the average of a quantity ϕ which we denote by $\langle\phi\rangle$. The fluctuation of ϕ is denoted by $\phi' \equiv \phi - \langle\phi\rangle$, and the root-mean-square variation of ϕ we denote by ϕ^{rms}. To obtain more reliable statistics, for each case we perform 25 repeated simulations using different seeds for the initial random field. Without further reference, all numerical results presented in this paper are ensemble averages of the DNS realizations.

The computational domain size is 10.472^2 (horizontally) $\times$ 6 (vertically) for which we use $128^2 \times 192$ grid points in our simulations. The timestep is 0.005. Based on the kinetic energy dissipation rate, the Kolmogorov length scale is estimated to be around 0.04, which is of the same order as the grid sizes ($\Delta_x = \Delta_y = 10.472/128 \simeq 0.08$; $\Delta_z = 6/192 \simeq 0.03$).

In order to ensure that all dynamically significant scales are resolved, we also carry out simulations using different grid sizes and timesteps. Figure 2(*a*) plots the relative errors of the mean velocity profile obtained with coarser resolutions relative to that using a fine resolution. It is shown that halving the grid size and timestep results in changes in the mean velocity profile of less than $O(1\%)$. All the results presented in

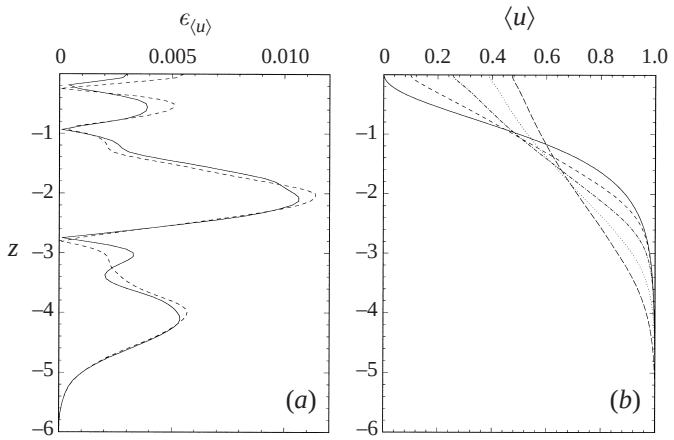

FIGURE 2. (*a*) Relative error in the mean velocity profile (at $t = 80$) $\varepsilon_{\langle u\rangle} \equiv |(\langle u\rangle_{lowres} - \langle u\rangle_{highres})/\langle u\rangle_{highres}|$ using a fine resolution of $128^2 \times 192$ grid points and timestep 0.005, compared to a lower resolution using $64^2 \times 96$ grid points and timestep: ————, 0.005; and – – – –, 0.01. (*b*) Time evolution of the mean velocity profile $\langle u\rangle(z)$ at: ————, $t = 0$; – – – –, 20; – · – · –, 40; · · · · · · ·, 60; — —, 80. The case plotted is for $Re_0 = 1000$ and $Fr_0 = 0.7$.

this paper are hereafter based on the fine spatial/temporal resolution given above. The time evolution of the mean velocity profile is plotted in figure 2(*b*) which shows, as expected, flattening of the mean shear with time (mainly) as a result of turbulent diffusion. The quantification of this development of the mean velocity in terms of profile shape and the associated time scaling behaviour is a main focus of this paper.

As a further validation, we consider the problem of the interaction between a small-amplitude two-dimensional progressive wave and the mean shear flow (3.1) under a free surface. We compare the direct simulation evolution to that obtained from an Orr–Sommerfeld stability analysis of this problem (see Zhang 1996, which is a viscous extension of Triantafyllou & Dimas 1989). Figure 3(*a*) plots the growth rate of the surface wave amplitude as a function of wavenumber. Figure 3(*b*) compares the time-evolution of this amplitude predicted from DNS to the Orr–Sommerfeld analysis for wavenumber 0.6 (which corresponds to the minimum wavenumber for the present DNS horizontal domain size of 10.472). The agreement is quite satisfactory.

Finally, we report that in all our simulations, the total kinetic energy is conserved to less than $O(1)\%$ error and the maximum mass divergence at any grid point is $O(10^{-14})$.

4. Numerical results

4.1. *Effects of the free-surface boundary conditions*

The zero-stress boundary conditions at the free surface influence quantities that involve derivatives of the velocity, for example the horizontal components of the vorticity. Using (2.6) and (2.5), we obtain the values of the two horizontal components of the vorticity at the free surface:

$$\omega_x = \frac{\partial w}{\partial y} - \frac{\partial v}{\partial z} = -2\frac{\partial v}{\partial z} = 2\frac{\partial w}{\partial y} \quad \text{on } z = 0, \tag{4.1}$$

$$\omega_y = \frac{\partial u}{\partial z} - \frac{\partial w}{\partial x} = 2\frac{\partial u}{\partial z} = -2\frac{\partial w}{\partial x} \quad \text{on } z = 0. \tag{4.2}$$

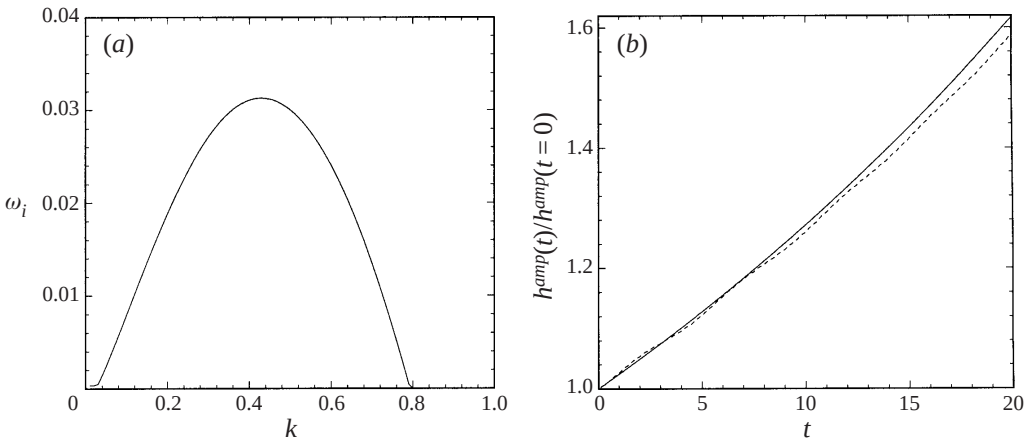

FIGURE 3. (*a*) Growth rate ω_i (the wave amplitude grows at the rate $\exp(\omega_i t)$) as a function of wavenumber k, obtained from Orr–Sommerfeld analysis of the mean flow (3.1) for $Re_0 = 1000$ and $Fr_0 = 0.7$. (*b*) Growth in amplitude of a two-dimensional surface progressive wave at wavenumber $k = 0.6$: ————, Orr–Sommerfeld analysis; – – – –, direct simulation result.

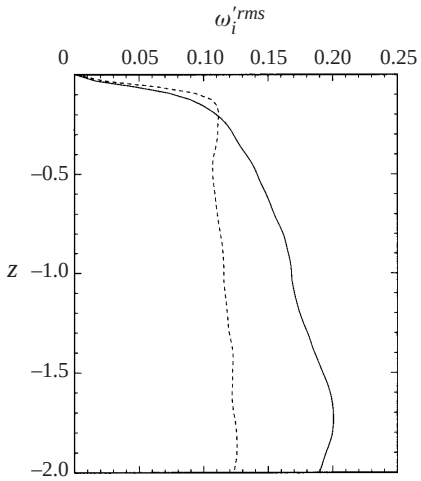

FIGURE 4. Vertical variation of $\omega_x'^{rms}$ (————) and $\omega_y'^{rms}$ (– – – –) at $t = 80$. $Re_0 = 1000$ and $Fr_0 = 0.7$.

The vertical velocity w is small at $z = 0$ owing to the constraint of the vertical motion at the free surface. It follows that ω_x and ω_y are small at $z = 0$. One thus expects that there exists a region over which ω_x and ω_y change from their bulk values to the small surface values. We denote this surface region the 'inner' layer. (The 'outer' layer will be introduced in §4.3.) The presence of this layer is shown clearly in the DNS results. Figure 4 plots the r.m.s. fluctuations of the horizontal vorticity components as functions of depth. The thin region of fast variations near the free surface defines the inner layer.

We remark that the presence of the inner layer in terms of velocity derivatives can also be identified in the results of previous free-surface turbulence studies, e.g. Leighton *et al.* (1991), Borue *et al.* (1995), Pan & Banerjee (1995), Walker *et al.* (1996), and Shen *et al.* (1999).

4.2. *The mean flow field*

Our present interest is the effects of the free-surface boundary layer(s) on the near-surface turbulent diffusion. To quantify these effects, the mean shear, rather than the mean velocity, is the main quantity of interest since the zero-stress boundary condition at the free surface requires it to vanish there.

For the mean (horizontally averaged) velocity, lateral symmetry of the problem obtains that $\langle v \rangle = 0$. Moreover, upon averaging (2.4), we obtain

$$\frac{\partial \langle w \rangle}{\partial z} = 0. \tag{4.3}$$

Far below the free surface, $\langle w \rangle \to 0$. Thus, $\langle w \rangle = 0$ everywhere.

Upon averaging the y-momentum equation (2.2) we obtain

$$\frac{\partial \langle v \rangle}{\partial t} + \frac{\partial (\langle v \rangle \langle w \rangle)}{\partial z} + \frac{\partial \langle v'w' \rangle}{\partial z} = \nu \frac{\partial^2 \langle v \rangle}{\partial z^2}. \tag{4.4}$$

Since $\langle v \rangle = \langle w \rangle = 0$ everywhere, we conclude that $\partial \langle v'w' \rangle / \partial z = 0$, and consequently that $\langle v'w' \rangle$ is constant. Far below the free surface $\langle v'w' \rangle \to 0$, therefore $\langle v'w' \rangle = 0$ everywhere. Thus the turbulent diffusion in the vertical direction is completely specified by the Reynolds stress $\langle -u'w' \rangle$.

Averaging the x-momentum equation (2.1) yields

$$\frac{\partial \langle u \rangle}{\partial t} + \frac{\partial \langle u'w' \rangle}{\partial z} = \nu \frac{\partial^2 \langle u \rangle}{\partial z^2}. \tag{4.5}$$

We define the eddy viscosity ν_e as usual:

$$\nu_e \equiv \frac{\langle -u'w' \rangle}{\partial \langle u \rangle / \partial z}. \tag{4.6}$$

We can now re-write (4.5) as follows:

$$\frac{\partial \langle u \rangle}{\partial t} = \frac{\partial}{\partial z} \left((\nu + \nu_e) \frac{\partial \langle u \rangle}{\partial z} \right). \tag{4.7}$$

Note that since the mean shear vanishes at the free surface (upon horizontal averaging of (2.5)):

$$\frac{\partial \langle u \rangle}{\partial z} = 0, \quad \text{on } z = 0; \tag{4.8}$$

equation (4.6) requires (for finite ν_e) that $\langle -u'w' \rangle$ also vanishes at $z = 0$. Applying l'Hopital's rule to (4.6), we obtain the limiting value of the eddy viscosity:

$$\nu_e|_{z=0} = \frac{\partial \langle -u'w' \rangle / \partial z|_{z=0}}{\partial^2 \langle u \rangle / \partial z^2|_{z=0}}. \tag{4.9}$$

The eddy viscosity is an even function of z, hence

$$\left. \frac{\partial \nu_e}{\partial z} \right|_{z=0} = 0. \tag{4.10}$$

Equation (4.9) gives, in general, a non-zero value of the eddy viscosity at the free surface, proportional to the flux of the momentum tensor at the free surface. In the

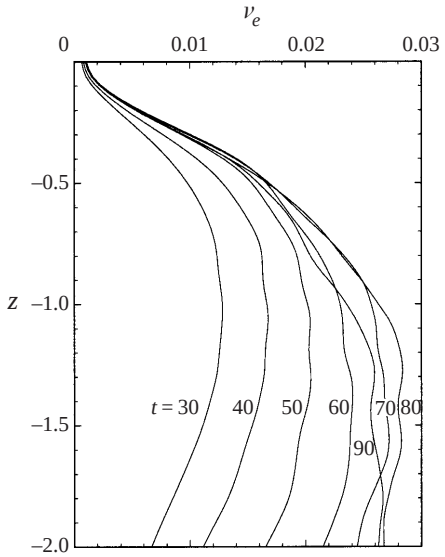

FIGURE 5. Profiles of eddy viscosity ν_e at different times. $Re_0 = 1000$ and $Fr_0 = 0.7$.

special case of a two-dimensional flow in the (x, z)-plane, where $v' = 0$, the right-hand side of (4.9) vanishes. In summary then, for a two-dimensional flow, we have

$$\nu_e|_{z=0} = \left.\frac{\partial \nu_e}{\partial z}\right|_{z=0} = 0. \tag{4.11}$$

4.3. *Quantitative definition of the free-surface boundary layer*

The thin inner layer of fast variation of the vorticity shown in figure 4 is not the only region that is influenced by the free surface (but it is the most obvious to see). There is a wider region which is also influenced by the surface. A good indicator of this is the variation of the eddy viscosity – far from the surface, the eddy viscosity reaches an almost constant value, whereas, close to the free surface, the eddy viscosity is reduced abruptly to its surface value. This free-surface 'outer' boundary layer (hereafter the 'outer' layer) can be seen in figures 5 and 6. Figure 5 shows the variation of the eddy viscosity with depth at various times and indicates the spatial extent of the outer layer. Figure 6 shows the variation of the eddy viscosity with time at various depths, and thus indicates the time required in our simulation for the boundary layer(s) to obtain the quasi-steady form ($t \gtrsim 60$ for $Re_0 = 1000$; this is also the case for $Re_0 = 700$ and 1400; these results are not plotted here).

The reduction of the eddy viscosity in a region near the free surface has also been seen in the measured data of Ueda *et al.* (1977) for open-channel flow. In that study, the value of the eddy viscosity at the free surface is assumed to be zero. This turns out to be not completely valid since the mixing length does not vanish at the free surface. The surface value of ν_e is, in fact, small and comparable to that of molecular viscosity ν. This is indicated from scaling arguments (see § 5.3) and is verified by our direct simulations. The value of ν_e at the free surface is exactly zero only in the limit of a strictly two-dimensional flow ($v = v' = 0$).

For later reference, we denote the thickness of the outer layer by ℓ_a, and the value of the eddy viscosity outside ℓ_a in the bulk of the flow by ν_{ea}. From dimensional

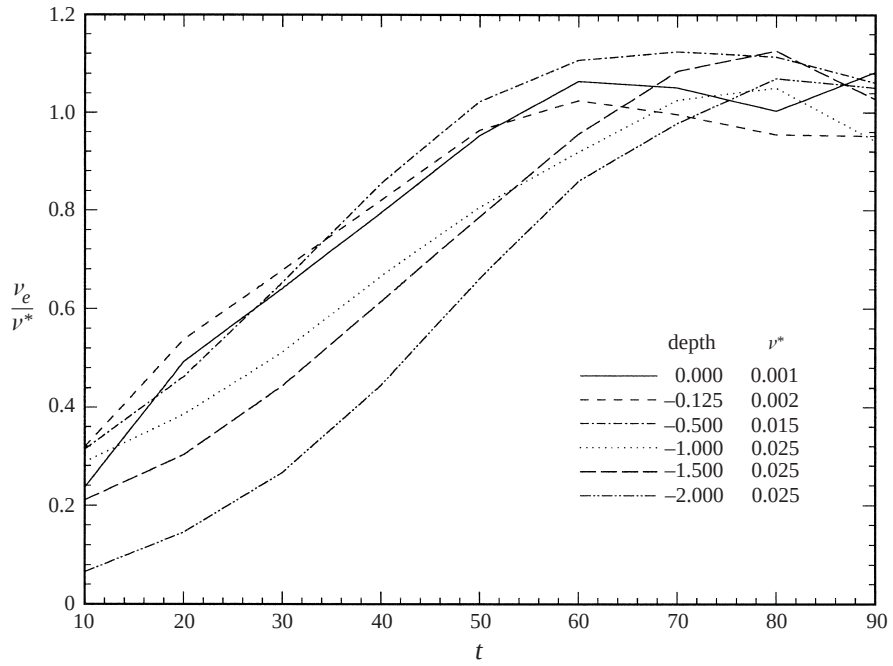

FIGURE 6. Time evolution of eddy viscosity ν_e at different depths. $Re_0 = 1000$ and $Fr_0 = 0.7$. Note that different scaling constants ν^* are used for different depths to allow the results to be fitted on the same plot.

analysis, a quantitative estimate for ℓ_a can be obtained and is given by

$$\ell_a^2 \sim \frac{2\nu_{ea}}{\partial^2 \nu_e / \partial z^2|_{z=0}}. \tag{4.12}$$

Another important observation here is the vertical variation of the mean shear over the free-surface boundary layer (see figure 7*a*). As the free surface is approached, the magnitude of the mean shear initially increases, and then drops rapidly to zero at the free surface. The magnitude of the mean shear thus exhibits two extrema near the free surface: a local minimum, and, much closer to the free surface, a local maximum.

The above features can be understood if we connect the depth variation of the mean shear to that of the eddy viscosity: inside the outer layer, the eddy viscosity decreases (figure 5) at a rate faster of that of the Reynolds stress (figure 7*b*). As a result, the magnitude of the mean shear is increased. Inside a much thinner inner layer, the mean shear then drops abruptly to zero in order to satisfy the zero-stress condition (4.8) at the free surface.

Based on this understanding, the thickness of the inner layer at the free surface can be defined as the distance from the free surface to the local maximum of the mean shear. Correspondingly, for the outer layer, the thickness can be defined as the distance of the local minimum of the mean shear from the free surface, which is physically more direct than the estimate (4.12) in terms of the curvature of ν_e at the free surface. Thus, with these definitions, the thicknesses of the surface layers can be obtained directly, for example, from an experimental determination of the mean velocity profile alone.

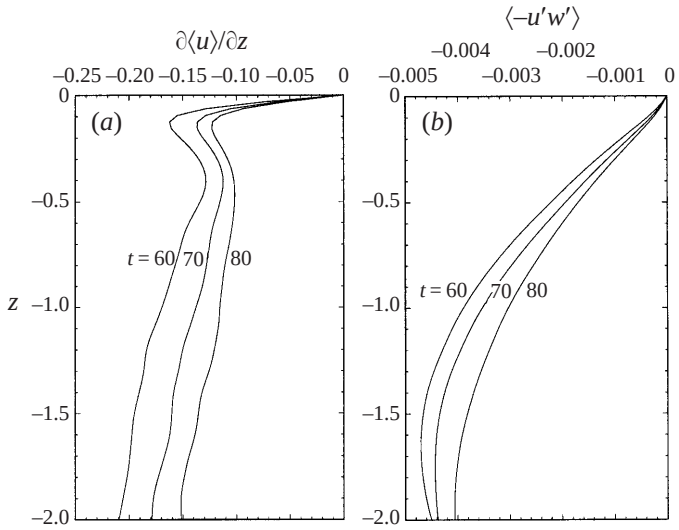

FIGURE 7. (*a*) Mean shear profiles $\partial\langle u\rangle/\partial z$; and (*b*) Reynolds stress profile $\langle -u'w'\rangle$ at different times. $Re_0 = 1000$ and $Fr_0 = 0.7$.

5. Analytical similarity solution

5.1. *Similarity solution*

From figure 5, one can observe that, at large times, the flow generally approaches a self-similar state: the temporal variation of the eddy viscosity in the bulk of the flow below is small, while the length scale of the spatial variation of the eddy viscosity increases with time. This suggests that one may look for a self-similar solution, say, of the form

$$\frac{U_\infty - \langle u\rangle}{U_d} = f(\eta), \tag{5.1}$$

where $U_\infty \equiv \langle u\rangle|_{z\to-\infty}$, $U_d = U_\infty - \langle u\rangle|_{z=0}$ is the velocity deficit, and η is the similarity variable

$$\eta = z/b, \tag{5.2}$$

with b measuring the extent of the mean shear in the flow. Note that both U_d and b are generally functions of time. This is done in order for the similarity solution to be comparable with the results of the simulation which refers to a temporally evolving flow. Extension of the similarity solution methodology to spatially evolving flows, which may better correspond to certain experimentally measured conditions, is straightforward and will not be done here.

The mean velocity $\langle u\rangle$ satisfies (4.7) subject to the boundary condition (4.8) on the free surface. For the eddy viscosity, it is important to take into account its variation with depth, in other words, the dependence of ν_e on U_d, b, the distance from the free surface z, and the molecular viscosity ν. Dimensional analysis then yields

$$\frac{\nu_e}{U_d b} = \psi\left(\eta; \frac{U_d b}{\nu}\right), \tag{5.3}$$

where ψ is some function of the similarity variable assumed known. We denote by ψ_a the value of ψ well below the free surface, i.e. outside the outer layer; and by ψ_0 the value of ψ at the free surface. One important point here is that near the free surface,

i.e. inside the outer layer, ψ should also depend on the Reynolds number, whereas far below the free surface, ψ should be independent of the Reynolds number.

Following the usual procedure (see e.g. Lesieur 1997), we find that U_d and b are related by

$$U_d b = C_0, \tag{5.4}$$

where C_0 is some constant. For the function $f(\eta)$, we find that it satisfies the ordinary differential equation

$$\eta f' + f = -\left(b\,\frac{\mathrm{d}b}{\mathrm{d}t}\right)^{-1} \frac{\mathrm{d}}{\mathrm{d}\eta}\left[(\nu + U_d b\psi)f'\right], \tag{5.5}$$

subject to the boundary conditions

$$f(0) = 1, \quad f'(0) = 0, \quad \text{and} \quad f'(-\infty) = 0. \tag{5.6}$$

It remains to specify the value of $f''(0)$. The appropriate choice can be made by writing (5.5) at $\eta = 0$:

$$(\nu + U_d b\psi_0)f''(0) = -b\frac{\mathrm{d}b}{\mathrm{d}t}. \tag{5.7}$$

The length b is the extent of the shear flow, which should be much greater than that of the outer layer. Consequently b should diffuse at a rate proportional to the value of the eddy viscosity in the bulk of the flow. This dictates the following choice:

$$f''(0) = -\frac{\nu + U_d b\psi_a}{\nu + U_d b\psi_0}, \tag{5.8}$$

and (5.7) becomes

$$b\frac{\mathrm{d}b}{\mathrm{d}t} = \nu + U_d b\psi_a. \tag{5.9}$$

Upon integration of (5.9), we obtain that b evolves in time as follows:

$$b = \sqrt{2(\nu + U_d b\psi_a)t + Q}, \tag{5.10}$$

where Q is a constant of integration. The velocity deficit U_d is given by

$$U_d = \frac{C_0}{\sqrt{2(\nu + U_d b\psi_a)t + Q}}. \tag{5.11}$$

Moreover by integrating (5.5) twice (subject to (5.6) and (5.8)) with respect to η we obtain the following expression:

$$f(\eta) = \exp\left(-\int_0^\eta \frac{s(\nu + U_d b\psi_a)}{\nu + U_d b\psi(s)}\mathrm{d}s\right). \tag{5.12}$$

Thus, we find that the length scale increases like the square root of t and the velocity deficit decreases at the inverse of this rate, as one may expect from a similarity solution. We note however that the choice (5.8) (which is based on physical reasoning) implies that $f''(0)$ is a large number since $\nu_{ea} = U_d b\psi_a$ is much greater than $\nu_{e0} \equiv \nu_e|_{z=0}$ and ν. Consequently $f'(\eta)$ has a region of fast variation in the vicinity of $\eta = 0$ which corresponds to the free-surface inner layer.

The similarity solution (5.12) provides us with a clear picture of the mean flow, and contains the basic physical features of interest. It remains to see how well it can fit the results of direct numerical simulation.

	$Re_0 = 700$			$Re_0 = 1000$			$Re_0 = 1400$		
t	U_d	b	C_0	U_d	b	C_0	U_d	b	C_0
60	0.680	1.529	1.040	0.612	1.669	1.021	0.602	1.684	1.014
65	0.644	1.617	1.041	0.587	1.744	1.024	0.575	1.753	1.008
70	0.621	1.683	1.045	0.566	1.815	1.027	0.557	1.816	1.012
75	0.591	1.768	1.045	0.544	1.874	1.019	0.536	1.880	1.008
80	0.566	1.853	1.049	0.527	1.939	1.022	0.518	1.939	1.004

TABLE 1. Variation with time of the mean velocity deficit U_d, the mean shear extent b, and the product $C_0 = U_d b$, for different Re_0.

5.2. *Comparison between theoretical similarity solution and direct simulations*

In order to compare (5.12) with the results of direct numerical simulations, we propose a simple Gaussian fit to the eddy viscosity (the validity of this particular choice will be subsequently supported by numerical results):

$$\psi = \frac{\nu_e}{U_d b} = \psi_a - (\psi_a - \psi_0)\exp(-\eta^2/a^2), \tag{5.13}$$

where a is proportional to the non-dimensional thickness of the outer layer (i.e. $a \sim \ell_a/b$). Using (5.13) we obtain from (5.12)

$$f(\eta) = \exp(-\eta^2/2)\left[\frac{1/Re + \psi_0}{1/Re + \psi_a - (\psi_a - \psi_0)\exp(-\eta^2/a^2)}\right]^{a^2/2}, \tag{5.14}$$

where Re is the Reynolds number based on U_d and b (note the difference from Re_0):

$$Re = \frac{U_d b}{\nu}. \tag{5.15}$$

Note that, because of (5.4), Re is independent of time for large time.

The eddy viscosity profile (5.13), the mean velocity profile (5.14) and its first derivative (i.e. the mean shear profile) are compared with results from direct numerical simulations after quasi-steady states are reached. The comparisons are performed as follows. The velocity deficit U_d is obtained directly from numerical results. The value of ψ_0 is obtained based on the eddy viscosity at the free surface; ψ_a is obtained based on the averaged eddy viscosity in the bulk of the flow; while b is determined by matching $f(\eta)$ in (5.14) with the numerical value at the depth $\eta = -1$, and the value of a is obtained by a least-square best fit of (5.13).

The values of U_d and b thus obtained at various times are listed in table 1. In agreement with (5.4), the product $C_0 = U_d b$ approaches a constant value at large times (the fluctuation in C_0 is less than 1% for $t \gtrsim 60$). Figure 8 shows the comparisons of the time evolution of U_d and b between the theoretical behaviour given by (5.10), (5.11) and that obtained from direct simulations (the values of C_0, ψ_a and Q used are listed in table 2). For the range of Reynolds numbers considered, the analytical solutions fit the computed behaviour of decreasing U_d and increasing b with time with remarkable accuracy.

Figure 9 compares the eddy viscosity given by (5.13) with DNS results at $t = 60$, 70, 80. There are small differences in the deep region, which can be attributed to the use of a constant eddy viscosity in the similarity solution there. Our main interest is the region near the free surface where figure 9 shows that the Gaussian profile (5.13)

Re_0	C_0	Re	ψ_a	ψ_0	v_{e0}/v	Q	a	$a(v/v_{ea})^{-1/2}$
700	1.04	728	0.0228	0.0014	1.05	−0.65	0.305	1.24
1000	1.02	1020	0.0229	0.00098	1.00	−0.14	0.251	1.21
1400	1.01	1414	0.0224	0.00078	1.10	−0.03	0.215	1.22

TABLE 2. Values of C_0, Re, ψ_a, ψ_0, v_{e0}/v, Q, a and $a(v/v_{ea})^{-1/2}$, for different Re_0.

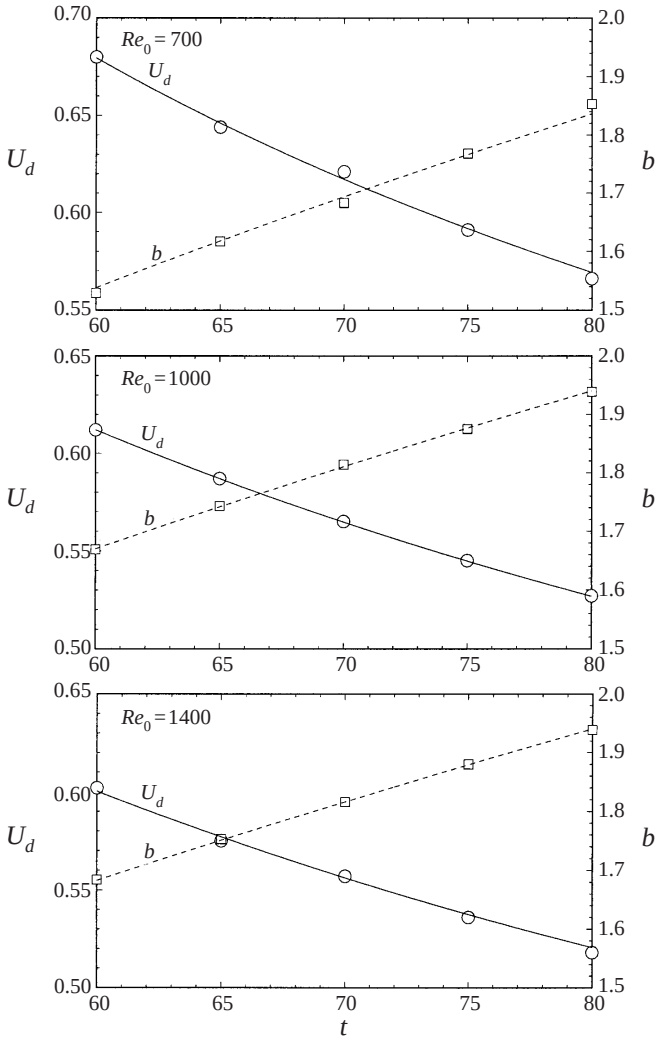

FIGURE 8. Time evolution of U_d and b for $Re_0 = 700$, 1000, and 1400 for: DNS results ($\circ$ for U_d, $\square$ for b; and similarity solution (———— for U_d, – – – – for b) .

fits the DNS v_e well in the near-surface region. As will be seen, (5.13) is sufficient to describe the detailed characteristics of the turbulent diffusion near the free surface.

Figure 10 shows similar comparisons for the mean velocity and figure 11 the mean shear rate. The agreement is quite good in both cases. (Note that small differences in the deeper region are due to the fact that the DNS turbulent flow underneath

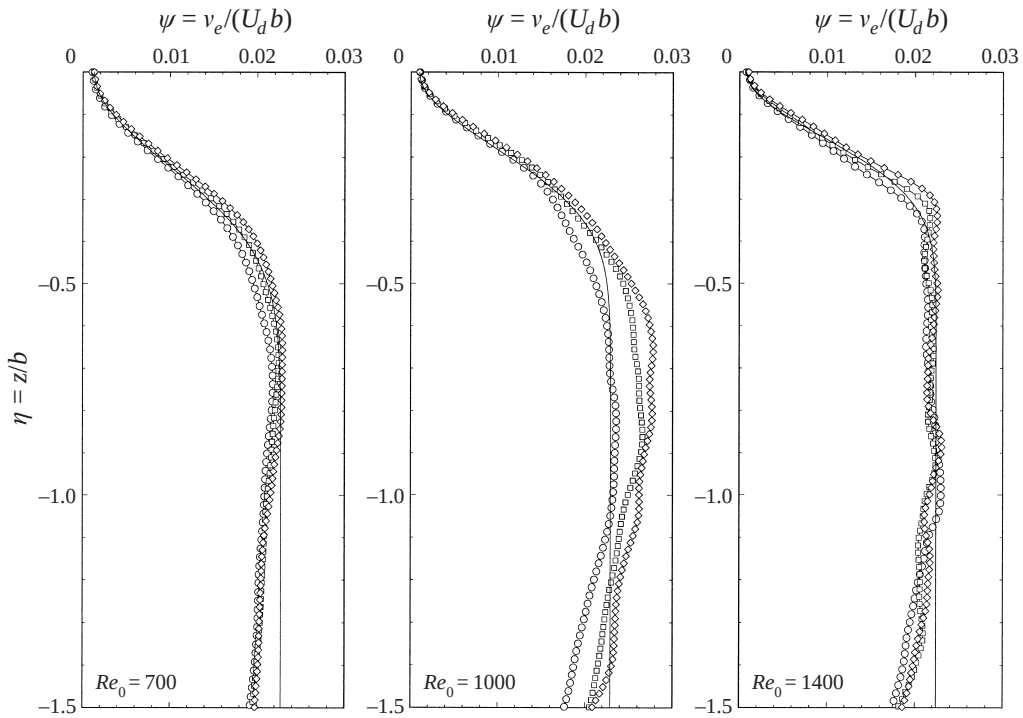

FIGURE 9. Comparison of the eddy viscosity profile between the similarity solution (————) and the DNS results at: ○, $t = 60$; □, $t = 70$; and ◇, $t = 80$; for $Re_0 = 700$, 1000, and 1400.

is not perfectly statistically homogeneous. Our main interest is in the near-surface region.) These two figures also confirm the similarity assumption that the mean flow approaches a universal shape at large times, although the physical values of the mean flow itself change with time (figures 2*b* and 7*a*).

5.3. *Scaling properties of the free-surface boundary layer*

As pointed out in § 5.1, one anticipates that the parameters a and ψ_0 should depend on the Reynolds number (since they describe properties of the outer layer), while ψ_a should be independent of the Reynolds number, as it describes the value of the eddy viscosity outside the outer layer. These are confirmed in table 2.

On the right-hand side of (5.14), the first (Gaussian) factor is what one would obtain in a constant eddy viscosity model, while the second factor is associated with the variation of eddy viscosity near the surface and, in particular, contains the essential information about the inner layer. Using a small-η ($\eta \ll a$) expansion of (5.14) we obtain

$$f(\eta) \approx \left[\frac{1/Re + \psi_0}{1/Re + \psi_0 + (\psi_a - \psi_0)\eta^2/a^2}\right]^{a^2/2} (1 - \eta^2/2). \tag{5.16}$$

Let ϵ be the non-dimensional thickness of the inner layer. Upon substitution of $\eta = \epsilon\zeta$ (with ζ being of order one) into (5.16), and using a dominant balance argument for the expression in the denominator of the right-hand side of (5.16), we obtain

$$\epsilon \sim a\left(\frac{1/Re + \psi_0}{\psi_a - \psi_0}\right)^{1/2}, \tag{5.17}$$

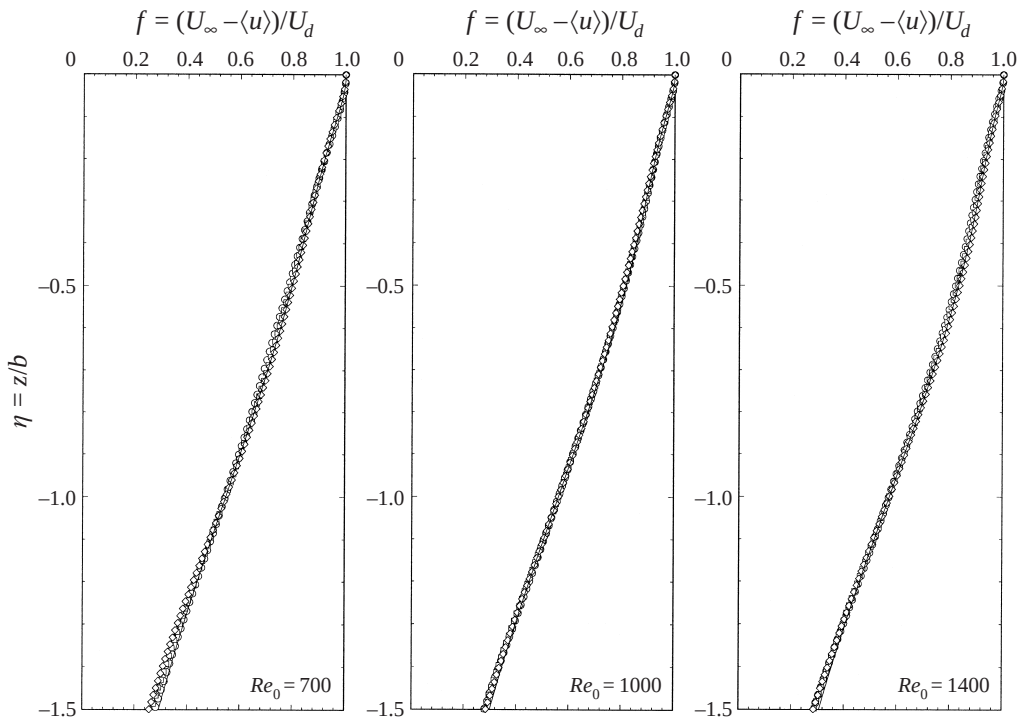

FIGURE 10. Comparison of the mean velocity profile between the similarity solution (————) and the DNS results at: ○, $t = 60$; □, $t = 70$; and ◇, $t = 80$; for $Re_0 = 700$, 1000, and 1400.

or equivalently,

$$\epsilon \sim a \left(\frac{\nu + \nu_{e0}}{\nu_{ea} - \nu_{e0}} \right)^{1/2}. \tag{5.18}$$

Equation (5.18) shows that the thickness of the inner layer, ϵ, is scaled by the thickness of the outer layer, a. It also shows that the value of the eddy viscosity at the free surface, ν_{e0}, enters into the estimate of the inner layer, and is therefore an important physical parameter of the problem.

We now turn to the dependence of ν_{e0} on the parameters of the problem. Based on (4.9), we can assume that the value of ν_{e0} depends on the following parameters: (i) the horizontal turbulence intensity at the free surface, q_0; (ii) the characteristic lateral size of the vortical structures attached on the free surface, λ_0; and (iii) the molecular viscosity, ν. It follows from dimensional analysis that

$$\frac{\nu_{e0}}{\nu} = F\left(Re_\lambda \equiv \frac{q_0 \lambda_0}{\nu} \right). \tag{5.19}$$

For a given free-surface shear-flow turbulence characterized by Re_λ, (5.19) indicates that the value of the eddy viscosity at the free surface scales like the value of the molecular kinematic viscosity. This fact is confirmed by our DNS data where the factor of proportionality between ν_{e0} and ν is found to be close to unity for a range of Re_0 (see table 2).

Interestingly, the similarity theory provides us also with a scaling relationship for the thickness of the outer layer. The estimate comes out in an indirect manner,

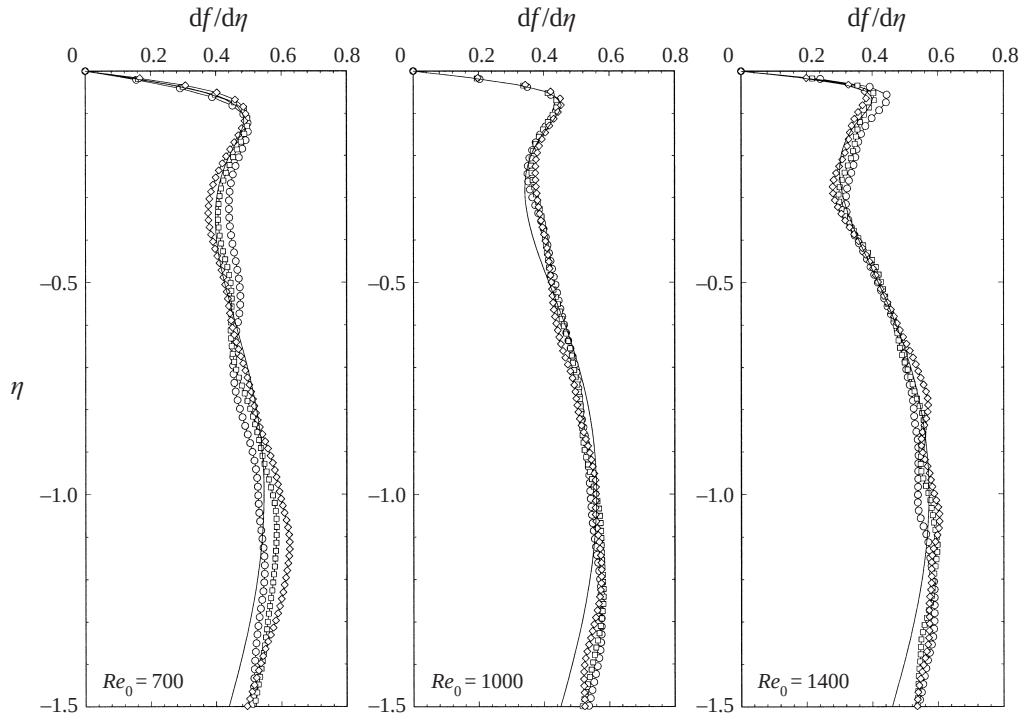

FIGURE 11. Comparison of the mean shear profile between the similarity solution (————) and the DNS results at: ○, $t = 60$; □, $t = 70$; and ◇, $t = 80$; for $Re_0 = 700$, 1000, and 1400.

through the requirement that the mean shear in the flow remains bounded at all Reynolds numbers.

Consistently with our discussion so far, and supported by DNS results, we assume that $\psi_a \gg 1/Re$, whereas ψ_0 is comparable to $1/Re$. Based on this and using the small-argument approximation, we find that the location of the maximum shear near the free surface is

$$\eta_m \approx -a\left[\frac{1/Re + \psi_0}{(1+a^2)\psi_a - \psi_0}\right]^{1/2}. \tag{5.20}$$

Therefore the maximum mean shear $s_m \equiv f'|_{max}$ is

$$s_m \approx a(Re\psi_a)^{1/2}\frac{(1+a^2-\psi_0/\psi_a)^{1/2}(1+(Re\psi_a)^{-1})}{(2+a^2-2\psi_0/\psi_a)(1+Re\psi_0)^{1/2}}. \tag{5.21}$$

Given that ψ_0 has the same order of magnitude as $1/Re$, we conclude that s_m remains bounded for $Re \to \infty$ only if $a(Re\psi_a)^{1/2}$ is at most order one, i.e. a is at most

$$a \sim (Re\psi_a)^{-1/2} = \left(\frac{\nu}{\nu_{ea}}\right)^{1/2}. \tag{5.22}$$

The decrease of the outer layer thickness as Reynolds number increases is evident in figures 9 and 11 for the DNS results. A more quantitative DNS confirmation is provided in table 2 which shows that the product $a(\nu/\nu_{ea})^{-1/2}$ is approximately constant.

It should be noted that the scaling relations (5.17) and (5.22) are not particular to

the eddy viscosity fitting (5.13). In fact they can be obtained directly from (5.12) by expanding $\psi(\eta)$ for small argument. Writing $\psi(\eta) = \psi_0 + \psi''(0)\eta^2/2 + \ldots$, and noting that in general the non-dimensional thickness of the outer layer a is proportional to $\psi_a/\psi''(0)$ (because of 4.12)), the derivation follows along the same lines as those we presented above.

Finally, we note that our DNS verification of the theoretical scaling results is limited to small Reynolds numbers. It would be very desirable to seek more complete/systematic numerical confirmation of these results. This is difficult primarily because of the fundamental limitations of DNS for high Reynolds numbers. Further examination using other approaches and especially experimental measurements would be helpful.

6. Implications for large-eddy simulation of free-surface turbulence

The understanding of the physics of turbulent diffusion near the free surface is essential to the modelling of free-surface turbulence (FST). In the preceding sections, we obtained the essential characteristics of free-surface turbulence and found that the averaged turbulence diffusion behaviour can be effectively described by a similarity solution. This understanding has immediate implications for modelling of free-surface turbulence in different contexts such as Reynolds-averaged Navier–Stokes (RANS) equations or large-eddy simulations (LES). In this section, we illustrate one such application in the development of a subgrid-scale (SGS) model for LES of free-surface turbulence.

In LES, the grid-scale motions are resolved while the subgrid-scale effects are modelled. For any variable $\phi(x, y, z)$, its grid-scale portion $\widehat{\phi}(x, y, z)$ is obtained by using a low-pass filter $G(x - \xi, y - \eta, z - \zeta)$:

$$\widehat{\phi}(x, y, z) = \int\int\int \phi(\xi, \eta, \zeta) G(x - \xi, y - \eta, z - \zeta)\, \mathrm{d}\xi\, \mathrm{d}\eta\, \mathrm{d}\zeta. \tag{6.1}$$

The governing equations for the grid-scale motions are

$$\frac{\partial \widehat{u}_k}{\partial x_k} = 0, \tag{6.2}$$

and

$$\frac{\partial \widehat{u}_i}{\partial t} + \frac{\partial \widehat{u}_i \widehat{u}_j}{\partial x_j} + \frac{\partial \tau_{ij}}{\partial x_j} = -\frac{\partial \widehat{p}}{\partial x_i} + \nu \frac{\partial^2 \widehat{u}_i}{\partial x_j \partial x_j}, \tag{6.3}$$

where τ_{ij} are the SGS stresses defined by

$$\tau_{ij} = \widehat{u_i u_j} - \widehat{u}_i \widehat{u}_j. \tag{6.4}$$

The SGS stresses reflect the contribution of SGS motions and are to be modelled as functions of grid-scale quantities. A commonly used model is the Smagorinsky model

$$\tau_{ij} = -2C_S \widehat{\Delta}^2 |\widehat{S}| \widehat{S}_{ij}, \tag{6.5}$$

where $\widehat{S}_{ij} \equiv (\partial \widehat{u}_i/\partial x_j + \partial \widehat{u}_j/\partial x_i)/2$, $|\widehat{S}| = (2\widehat{S}_{ij}\widehat{S}_{ij})^{1/2}$, $\widehat{\Delta}$ is the grid filter width, and C_S is the Smagorinsky coefficient to be determined.

In the present problem, the horizontal plane is statistically homogeneous and we assume that the Smagorinsky coefficient is a function of depth and time only, i.e. $C_S = C_S(z, t)$. The key to the success of the LES is to correctly capture the spatial variation of the Smagorinsky coefficient near the free surface. Based on the findings

of the preceding sections, we propose a *free-surface function model* (FFM) for the SGS stresses. In this model, we simply assume that C_S has similar behaviour to the turbulence diffusivity:

$$C_S(z,t) = C_{Sa} - (C_{Sa} - C_{S0}) \exp\,[-(z/\ell^S(t))^2], \tag{6.6}$$

where C_{Sa} and C_{S0} are respectively the values of C_S in the bulk and at the free surface, and ℓ^S is the (time-dependent) length scale of the variation of the Smagorinsky coefficient.

To evaluate the validity of the FFM (6.6), we first perform *a priori* tests (cf. Clark, Ferziger & Reynolds 1979; McMillan, Ferziger & Rogallo 1980) wherein the right-hand side of (6.5) is evaluated and compared to (6.4) using a DNS dataset (where all the scales are solved). To do this, we apply a Gaussian grid filter (Kwak, Reynolds & Ferziger 1975) in the (periodic) horizontal directions and a discrete grid filter in the vertical direction given by

$$G(x-\xi, y-\eta, z-\zeta) = G_1(x-\xi)G_2(y-\eta)G_3(z-\zeta), \tag{6.7}$$

$$G_1(x-\xi) = (6/\pi)^{1/2} \exp\,[-6(x-\xi)^2/\widehat{\Delta}_x^2], \tag{6.8}$$

$$G_2(y-\eta) = (6/\pi)^{1/2} \exp\,[-6(y-\eta)^2/\widehat{\Delta}_y^2], \tag{6.9}$$

$$G_3(z-\zeta) = [\delta(z-\zeta-\widehat{\Delta}_z) + 2\delta(z-\zeta) + \delta(z-\zeta+\widehat{\Delta}_z)]/4. \tag{6.10}$$

Here δ is the Dirac function; $\widehat{\Delta}_x$ (= 0.6545), $\widehat{\Delta}_y$ (= 0.6545) and $\widehat{\Delta}_z$ (= 0.0625) are the filter widths in the x-, y- and z- directions, respectively and the overall filter width is given by $\widehat{\Delta} \equiv (\widehat{\Delta}_x\widehat{\Delta}_y\widehat{\Delta}_z)^{1/3}$ (= 0.2992).

Figure 12 plots the horizontally averaged C_S obtained from (6.5) using DNS data for the $Re_0 = 1400$ case of § 4 compared to that given by (6.6). The best fit values for the model parameters in figure 12 are $C_{Sa} \approx 0.019$ (a value in agreement with those found in shear flow turbulence, cf. Rogallo & Moin 1984; Lesieur & Metais 1996), $C_{S0} \approx 0.003$, and $\ell^S/a \approx 0.6$. The decrease of C_S towards the free surface is consistent with the results of the preceding sections, and the fit to the Gaussian profile is quite acceptable.

We now proceed with *a posteriori* tests of the FFM. In these tests, the SGS model is used directly in LES and the results then compared to higher resolution DNS. For the LES, we use a coarse $32^2 \times 96$ grid (the DNS grid is $128^2 \times 192$). For the initial condition, we use DNS data at $t = 60$ filtered by (6.7). The LES results are compared to filtered DNS data after dimensionless time 10 at $t = 70$.

Figure 13 evaluates the *a posteriori* performance of LES using FFM. For the intensity of the (grid-scale) turbulence fluctuation $\widehat{q}^2 \equiv \widehat{u}'^2 + \widehat{v}'^2 + \widehat{w}'^2$ (figure 13*a*), the comparison between the FFM and DNS profiles is excellent. Also shown is the result when a constant Smagorinsky coefficient (say, given by its bulk value) is used. In this case, the turbulence intensity in the near-surface region is over damped, as expected, since the constant Smagorinsky coefficient is unable to capture the decaying turbulent diffusion towards the free surface. For reference, we also plot in figure 13(*a*) the result when no SGS model is used in the coarse-grid simulation. Without the SGS stresses, the prediction is clearly inadequate. Similar results and conclusions obtain also for the mean (grid-scale) shear rate as shown in figure 13(*b*).

These results show that, by capturing the turbulence diffusion behaviour of free-surface turbulence, the FFM provides an effective SGS model for LES of free-surface turbulence. We remark finally that the FFM extends in a straightforward way to

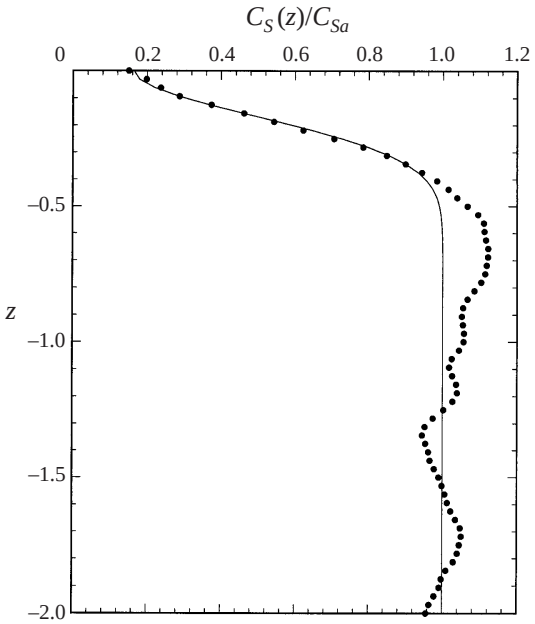

FIGURE 12. Vertical variation of the Smagorinsky coefficient C_S: •, horizontally averaged values using DNS and (6.5); ————, fitted curve given by (6.6). $Re_0 = 1400$ and $t = 70$.

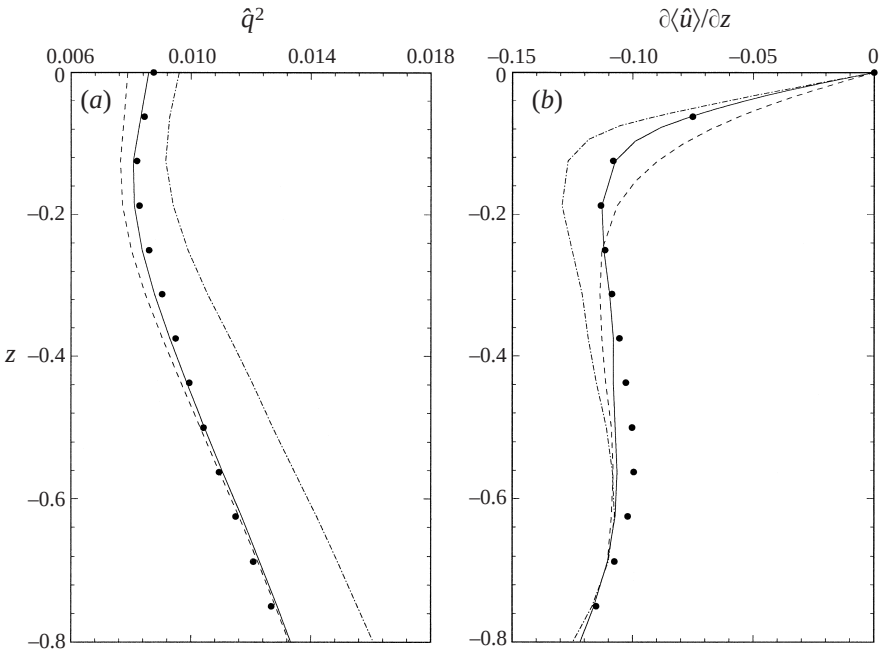

FIGURE 13. *A posteriori* test results for (*a*) (grid-scale) turbulence intensity $\widehat{q}^2$ and (*b*) mean (grid-scale) shear rate $\partial\langle\widehat{u}\rangle/\partial z$, •: DNS results; and (coarse-grid) LES results using: ————, free-surface function model (FFM); – – – –, constant-coefficient Smagorinsky model; – · – · –, no model. $Re_0 = 1400$ and $t = 70$.

dynamic LES schemes (Germano *et al.* 1991). For free-surface turbulence, the dynamic schemes (DTM) of Salvetti & Banerjee (1995) and Salvetti *et al.* (1997) have been shown to capture the anisotropy and SGS energy transfer near the free surface. Whether models such as the FFM can provide further improvements is clearly of interest. The Germano-dynamic and other extensions of FFM and a detailed evaluation of the results are subjects of a follow-up paper.

7. Conclusions

In this paper we investigate the process of turbulent diffusion in a shear flow under a free surface. We obtain an ensemble of simulation results using DNS. Using these data, we identify the free-surface boundary layer structures: an outer layer characterized by the reduction of the eddy viscosity and an accompanying increase of the mean shear rate; and an inner layer characterized by the rapid decrease of the mean shear rate to reach its vanishing value at the free surface. We find that quantitative definitions of the outer and inner thicknesses can be obtained directly from the mean shear profile corresponding respectively to first its local minimum and then its local maximum as the free surface is approached.

Guided by DNS results, we derive a similarity theory for the vertical turbulent diffusivity problem. An important feature of the similarity solution is the specification of a universal shape for the mean velocity profile. This and other predictions of the similarity theory are confirmed by direct comparisons to DNS. Significantly, the similarity solution provides the scaling for the thickness of the inner and outer surface layers as a function of the Reynolds number: the inner layer thickness is proportional to the outer layer thickness; the outer layer thickness is proportional to the mean shear depth; and the factors of proportionality in both cases scale as the square root of the ratio of the molecular viscosity to the bulk eddy viscosity. Thus, the free-surface boundary layers define the region of the flow which remains Reynolds number dependent at high Reynolds numbers.

The above results provide a fundamental basis for the modelling of turbulence at a free surface. As an illustration, we propose a free-surface function model (FFM) for large-eddy simulation of free-surface turbulence. This new model incorporates the expected near free-surface behaviour of the turbulence diffusivity and is an improvement over classical models using constant coefficients. This is borne out by *a priori* and *a posteriori* tests against DNS.

We remark that the concept of free-surface boundary layer(s) itself is not new (see § 1). In a previous study (Shen *et al.* 1999), we identified at the free surface an inner 'surface' layer and an outer 'blockage' layer. The inner 'surface' layer in Shen *et al.* (1999) is closely related to the inner layer here – both are direct results of the vanishing tangential stress condition at the free surface. The former was established based on vanishing vorticity components at the surface, while in the present work, the inner layer is quantified by the mean shear rate which vanishes at the surface.

The 'blockage' layer of Shen *et al.* (1999) is a kinematic consequence of the boundary condition at the free surface. This kinematic 'blockage' layer is obtained only qualitatively and, from continuity, has a thickness of the order of the integral scale. The present outer layer, on the other hand, is a direct measure of the region over which turbulence diffusivity is affected by the presence of the free surface. As such, the thickness of this outer layer is a function of Reynolds number (given by (5.22)). In terms of the dynamics of free-surface turbulence, the present notion of the

free-surface inner and outer layers provides an important understanding and model of the near-surface turbulent flow.

Finally, with the more comprehensive picture of the free-surface layers obtained from this and previous work, it is instructive to compare the inner/outer free-surface layer structure found here to the structure of the boundary layer at a solid wall. In both cases there is an inner layer much thinner than the outer one. Within this inner layer diffusion is due predominantly to viscosity which determines the scaling of its thickness. There exists an important difference between the two however. At the solid wall, fluid motion in all directions vanishes, energy dissipation is large inside the wall boundary layer, and the flow becomes laminar close enough to the wall. In contrast, the free surface restricts motion in the normal direction only. Inside the (inner) free-surface boundary layer, energy dissipation is reduced as a result of the zero-stress surface condition, and horizontal velocity fluctuations in fact increase towards the surface.

This research was financially supported by the Office of Naval Research under the program management of Dr E. P. Rood.

REFERENCES

Borue, V., Orszag, S. A. & Staroselsky, I. 1995 Interaction of surface waves with turbulence: direct numerical simulations of turbulent open-channel flow. *J. Fluid Mech.* **286**, 1–23.

Clark, R. A., Ferziger, J. H. & Reynolds, W. C. 1979 Evaluation of subgrid-scale models using an accurately simulated turbulent flow. *J. Fluid Mech.* **91**, 1–16.

Davis, J. T. 1972 *Turbulence Phenomena*. Academic.

Dimas, A. A. & Triantafyllou, G. S. 1994 Nonlinear interaction of shear flow with a free surface. *J. Fluid Mech.* **260**, 211–246.

Dimas, A. A. & Triantafyllou, G. S. 1995 Numerical study of Langmuir circulations in turbulent shear flows with a free surface. *Proc. 10th Symp. on Turbulent Shear Flows*, vol. 3, pp. 27 : 1–12. Pennsylvania State University.

Ellison, T. H. 1960 A note on the velocity profile and longitudinal mixing in a broad open channel. *J. Fluid Mech.* **8**, 33–40.

Germano, M., Piomelli, U., Moin, P. & Cabot, W. H. 1991 A dynamic subgrid-scale eddy viscosity model. *Phys. Fluids* A **3**, 1760–1765.

Gharib, M., Dabiri, D. & Zhang, X. 1994 Interaction of small scale turbulence with a free surface. In *Free-Surface Turbulence* (ed. E. P. Rood & J. Katz), pp. 97–102. ASME.

Handler, R. A., Swean, T. F. Jr., Leighton, R. I. & Swearingen, J. D. 1991 Length scales of turbulence near a free surface. *AIAA Paper* 91-1775.

Handler, R. A., Swean, T. F. Jr., Leighton, R. I. & Swearingen, J. D. 1993 Length scales and the energy balance for turbulence near a free surface. *AIAA J.* **31**, 1998–2007.

Harlow, F. H. & Welch J. E. 1965 Numerical calculation of time-dependent viscous incompressible flow of fluid with free surface. *Phys. Fluids* **8**, 2182–2189.

Hunt, J. N. 1954 The turbulent transport of suspended sediment in open channels. *Proc. R. Soc. Lond.* A **224**, 322–335.

Jobson, H. E. & Sayre, W. W. 1970 Vertical transfer in open channel flow. *J. Hydraul. Div. ASCE* **96**, 703–724.

Komori, S., Murakami, Y. & Ueda, H. 1989 Detection of coherent structures associated with bursting events in an open-channel flow by a two-point LDV-measuring technique. *Phys. Fluids* A **1**, 339–348.

Komori, S., Ueda, H., Ogino, F. & Mizushina, T. 1982 Turbulence structure and transport mechanism at the free surface in an open channel flow. *Intl J. Heat Mass Transfer* **25**, 513–521.

Kwak, D., Reynolds, W. C. & Ferziger, J. H. 1975 Three dimensional time dependent computation of turbulent flows. *Rep.* TF-5. Mech. Engng Dept., Standford University.

Lam, K. & Banerjee, S. 1988 Investigation of turbulent flow bounded by a wall and a free surface. In *Fundamentals of Gas-Liquid Flows* (ed. E. Michaelides & M. P. Sharma), pp. 29–38. ASME.

Lee, G. Y. & Gill, W. N. 1977 A note on velocity and eddy viscosity distributions in turbulent shear flows with free surfaces. *Chem. Engng Sci.* **32**, 967–969.

Leighton, R. I., Swean, T. F., Handler, R. A. & Swearingen, J. D. 1991 Interaction of vorticity with a free surface in turbulent open channel flow. *AIAA Paper* 91-0236.

Lesieur, M. 1997 *Turbulence in Fluids*. Kluwer.

Lesieur, M. & Metais, O. 1996 New trends in large-eddy simulations of turbulence. *Ann. Rev. Fluid. Mech.* **28**, 45–82.

Levich, V. G. 1962 *Physiochemical Hydrodynamics*. Prentice-Hall.

Mattingly, G. E. & Criminale, W. O. 1972 The stability of an incompressible two-dimensional wake. *J. Fluid Mech.* **51**, 233–272.

McMillan, O. J., Ferziger, J. H. & Rogallo, R. S. 1980 Tests of new subgrid-scale models in strained turbulence. *AIAA Paper* 80-1339.

Nakagawa, H. & Nezu, I. 1981 Structure of space-time correlation of bursting phenomena in an open channel flow. *J. Fluid Mech.* **104**, 1–43.

Pan, Y. & Banerjee, S. 1995 A numerical study of free-surface turbulence in channel flow. *Phys. Fluids* **7**, 1649–1664.

Perot, B. & Moin, P. 1995 Shear-free turbulent boundary layers. Part 1. Physical insights into near-wall turbulence. *J. Fluid Mech.* **295**, 199–227.

Rashidi, M. 1997 Burst-interface interactions in free surface turbulent flows. *Phys. Fluids* **9**, 3485–3501.

Rashidi, M. & Banerjee, S. 1988 Turbulence structure in free surface channel flows. *Phys. Fluids* **31**, 2491–2503.

Rashidi, M. & Banerjee, S. 1990 The effects of boundary conditions and shear rate on streak formation and breakdown in turbulent channel flows. *Phys. Fluids* A **32**, 1827–1838.

Rogallo, R. S. & Moin, P. 1984 Numerical simulation of turbulent flows. *Ann. Rev. Fluid. Mech.* **16**, 99–137.

Salvetti, M. V. & Banerjee, S. 1995 *A priori* tests of a new dynamic subgrid-scale model for finite-difference large-eddy simulations. *Phys. Fluids* **7**, 2831–2847.

Salvetti, M. V., Zang, Y., Street, R. L. & Banerjee, S. 1997 Large-eddy simulation of free-surface decaying turbulence with dynamic subgrid-scale models. *Phys. Fluids* **9**, 2405–2419.

Shen, L., Zhang, X., Yue, D. K. P. & Triantafyllou, G. S. 1999 The surface layer for free-surface turbulent flows. *J. Fluid Mech.* **386**, 167–212.

Swean, T. F. Jr., Leighton, R. I., Handler, R. A. & Swearingen, J. D. 1991 Turbulence modelling near the free surface in open cannel flow. *AIAA Paper* 91-0613.

Triantafyllou, G. S. & Dimas, A. A. 1989 Interaction of two-dimensional separated flows with a free surface at low Froude numbers. *Phys. Fluids* A **1**, 1813–1821.

Ueda, H., Moller, R., Komori, S. & Mizushina, T. 1977 Eddy diffusivity near the free surface of open channel flow. *Intl J. Heat Mass Transfer*. **20**, 1127–1136.

Walker, D. T., Leighton, R. I. & Garza-Rios, L. O. 1996 Shear-free turbulence near a flat free surface. *J. Fluid Mech.* **320**, 19–51.

Zhang, C. 1996 Turbulent free-surface wakes behind towed model – experimental measurements, numerical simulations and stability analysis. PhD thesis, Department of Ocean Engineering, MIT.